The Astrophysical Journal Letters, 956:L44 (6pp), 2023 October 20 https://doi.org/10.3847/2041-8213/acff60

Unveiling the Nature of Galactic TeV Sources with IceCube Results

V. Vecchiotti[1], F. L. Villante[2,3], and G. Pagliaroli[3]
[1] Norges Teknisk-naturvitenskapelige Universitet, Department of Physics, NO-7491 Trondheim, Norway; vittoria.vecchiotti@ntnu.no
[2] University of L'Aquila, Physics and Chemistry Department, I-67100 L'Aquila, Italy
[3] Istituto Nazionale di FIsica Nucleare, Laboratori Nazionali del Gran Sasso, I-67100 Assergi (AQ), Italy
Received 2023 July 20; revised 2023 September 20; accepted 2023 September 28; published 2023 October 20

Abstract

IceCube collaboration reported the first high-significance observation of the neutrino emission from the Galactic disk. The observed signal can be due to diffuse emission produced by cosmic rays interacting with interstellar gas but can also arise from a population of sources. In this paper, we evaluate both the diffuse and source contribution by taking advantage of gamma-ray observations and/or theoretical considerations. By comparing our expectations with IceCube measurements, we constrain the fraction of Galactic TeV gamma-ray sources (resolved and unresolved) with hadronic nature. In order to be compatible with the IceCube results, this fraction should be small, or the source proton energy cutoff should be well below the cosmic-ray proton knee. In particular, for a cutoff energy equal to 500 TeV, the fraction of hadronic sources should be less than ∼40% corresponding to a cumulative source flux $\Phi_{\nu,s} \leqslant 2.6 \times 10^{-10}\,\mathrm{cm}^{-2}\,\mathrm{s}^{-1}$ integrated in the 1–100 TeV energy range. This fraction reduces to ∼20% for energy cutoff reaching the cosmic-ray proton knee around 5 PeV.

Unified Astronomy Thesaurus concepts: Neutrino astronomy (1100); High-energy cosmic radiation (731)

1. Introduction

The diffuse Galactic neutrino emission produced by hadronic interactions of high-energy cosmic rays (CRs) with the gas contained in the Galactic disk is a guaranteed signal for neutrino telescopes (Evoli et al. 2007; Pagliaroli et al. 2016; Lipari & Vernetto 2018; Cataldo et al. 2019; Schwefer et al. 2023). The detection of this component is, however, challenging due to both the atmospheric neutrino background and to its subdominant role in all-sky astrophysical neutrino emission (Adrian-Martinez et al. 2016; Aartsen et al. 2017; Albert et al. 2017, 2018, 2023). Very recently, IceCube succeeded in its detection thanks to a decade of accumulated statistics and exploiting new machine-learning techniques, providing the first detection of the neutrino emission from the Galactic plane at the 4.5σ level of significance (Abbasi et al. 2023). IceCube exploits a template-fitting procedure, testing the data compatibility with three models for the expected Galactic diffuse neutrino emission. For each model, the spatial and spectral shapes are frozen to the expected ones, while the normalization is free to match the neutrino data considering the entire sky.

All the models considered by IceCube describe the truly diffuse emission expected by CR interactions with the interstellar medium. However, freshly accelerated hadrons colliding with the ambient medium within or close to an acceleration site can also produce high-energy neutrinos; see, e.g., Ahlers & Murase (2014). This "sources" component cannot be resolved with the actual statistics and with the poor angular resolution of IceCube cascade events, providing an additional large-scale Galactic neutrino emission that adds to the truly diffuse emission due to CR interactions. The detected IceCube neutrino signal is most likely due to the total Galactic neutrino emission where part of the signal could also arise from a population of unresolved point sources, as also stated by the IceCube collaboration.

In this paper, we discuss the relative importance of truly diffuse and source components by using a multi-messenger approach. High-energy sources have been observed in the TeV and sub-PeV energy domain by gamma-ray detectors, such as H.E.S.S. (Abdalla et al. 2018), HAWC (Albert et al. 2020), and LHAASO (Cao et al. 2023). It was recently proven that unresolved gamma-ray sources have a relevant role in the interpretation of the large-scale gamma-ray emission detected in different energy ranges. In particular, the presence of an unresolved source component at ∼10 GeV added to the truly diffuse emission can change the spectral shape of the diffuse gamma-ray signal observed by Fermi Large Area Telescope (-LAT), mimicking a CR's spectral hardening in the inner Galaxy (Vecchiotti et al. 2022a). At very high energy, the presence of the additional diffuse component due to unresolved sources seems needed to obtain a good agreement with the Tibet ASγ data, especially at high longitudes (Fang & Murase 2021; Vecchiotti et al. 2022b). All this suggests that sources could give a non-negligible contribution also to neutrino emission in the TeV energy domain explored by IceCube. The relevance of this component depends, however, on the hadronic or leptonic nature of sources. Hadronic processes produce a roughly equal number of charged and neutral pions that decay to neutrinos and gamma rays, respectively. This strong correlation between the neutrino and gamma-ray sky, always valid for the truly diffuse emission, fails for the "sources" component if they have a leptonic nature. In the following, we discuss the constraints on the fraction of Galactic TeV gamma-ray sources (resolved and unresolved) with hadronic nature that can be obtained from IceCube results.

2. Results

The signal observed by IceCube is determined by the total Galactic neutrino emission:

$$\varphi_{\nu,\mathrm{tot}}(E_\nu;\, E_{\mathrm{cut}},\, \xi) = \varphi_{\nu,\,\mathrm{diff}}(E_\nu) + \varphi_{\nu,s}(E_\nu;\, E_{\mathrm{cut}},\, \xi), \qquad (1)$$

which is obtained as the sum of the truly diffuse emission $\varphi_{\nu,\mathrm{diff}}$ produced by CR interactions with the interstellar gas and the cumulative contribution produced by sources $\varphi_{\nu,s}$ within a given observation window. Since sources cannot be individually resolved, the two components cannot be disentangled unless one uses additional information provided by gamma-ray observations and/or theoretical considerations, as is done in this paper. The diffuse component can be estimated by using the approach described in Pagliaroli et al. (2016) and Cataldo et al. (2019); see Appendix A. The obtained predictions depend on the assumed CR spatial and energy distribution, motivating the two cases (labeled as "Case B" and "Case C", respectively) discussed more in detail in the following sections. The cumulative neutrino source flux $\varphi_{\nu,s}(E_\nu; E_{\mathrm{cut}}, \xi)$ is calculated by using the approach described in Vecchiotti et al. (2023), which relies on the population study of the sources in the H.E.S.S. Galactic plane survey (HGPS) catalog (Abdalla et al. 2018) performed by Cataldo et al. (2020); see Appendix B and Appendix C. It is obtained by assuming that a fraction ξ of the source population emits gamma rays and neutrinos due to hadronic interactions of primary nucleon flux $\phi_{\mathrm{p}}(E) \propto E^{-\Gamma_{\mathrm{p}}} \exp(-E/E_{\mathrm{cut}})$. In our calculations, the proton spectral index is chosen as $\Gamma_p = 2.4$ to reproduce the average spectral properties of HGPS sources, while the proton cutoff energy E_{cut} is free to vary. The source component is thus obtained in terms of two parameters, ξ and E_{cut}, and can be written as

$$\varphi_{\nu,s}(E_\nu; E_{\mathrm{cut}}, \xi) = \xi\, \Phi^{\mathrm{max}}_{\nu,s}(E_{\mathrm{cut}})\, \phi_\nu(E_\nu; E_{\mathrm{cut}}), \qquad (2)$$

where $\Phi^{\mathrm{max}}_{\nu,s}$ represents the maximal source neutrino flux integrated in the [1, 100] TeV energy window, i.e., the neutrino source contribution obtained by assuming that all the TeV gamma-ray sources, resolved and unresolved, are powered by hadronic processes. For $E_{\mathrm{cut}} \geqslant 500$ TeV, the maximal source neutrino flux, integrated in the observational window (OW) $|b| < 5^\circ$ and $0^\circ \leqslant l \leqslant 360^\circ$ considered in this work, is equal to $\Phi^{\mathrm{max}}_{\nu,s} = 6.4 \times 10^{-10}\,\mathrm{cm^{-2}\,s^{-1}}$ within 10% accuracy. The quantity $\phi_\nu(E_\nu; E_{\mathrm{cut}})$ is the neutrino spectrum produced by hadronic interactions (normalized in the same energy window); see Appendix C for details. By choosing $\xi = 1$ and $E_{\mathrm{cut}} = \infty$, we are able to determine the maximal neutrino flux allowed by gamma-ray observation. It should be noted that this limit, being based on the entire population of gamma-ray sources, includes by construction also the potential contribution of sources that are not resolved by present gamma-ray telescopes. A neutrino signal larger than this upper limit can only be obtained by requiring the presence of hadronic source opaque in gamma rays.

In Figures 1 and 2 we compare our predictions for the Galactic neutrino emission with the IceCube results. The IceCube Galactic signal is obtained by using a template-fitting procedure where the angular and energy dependence of the neutrino flux is fixed according to three different models, namely the π_0 (Ackermann et al. 2012), KRA^5_γ, and KRA^{50}_γ models (Gaggero et al. 2015), while the overall normalization is free to vary. We restrict our comparison to the angular region $0^\circ \leqslant l \leqslant 360^\circ$ and $|b| < 5^\circ$ where the best fits of the Galactic neutrino component obtained for the different templates give

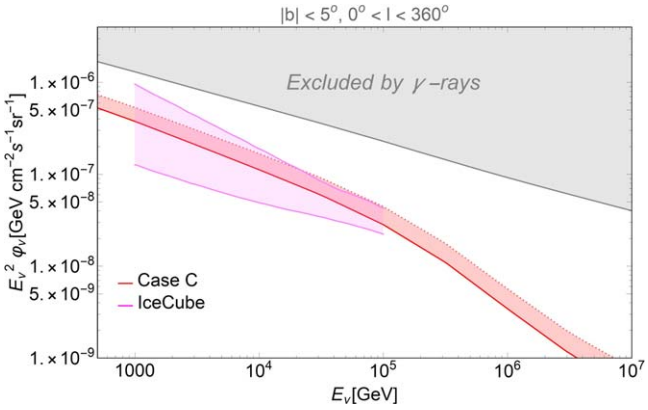

Figure 1. Differential energy spectra of the all-flavor diffuse neutrino emission from the Galactic region $|b| < 5^\circ$ and $0^\circ < l < 360^\circ$. The magenta region corresponds to the superposition of the three IceCube best fits for the Galactic component with their 1σ uncertainty. The prediction for the diffuse emission (Case C) is shown with a red band. The bands represent the uncertainties on the spatial distributions of CRs in our Galaxy. The solid and dotted lines are obtained by assuming smearing radius infinity and 1 kpc, respectively. We additionally display an excluded region in gray. The bottom line corresponds to the maximum neutrino contribution from our Galaxy obtained by assuming Case C for the diffuse emission, $\xi = 1$ and $E_{\mathrm{cut}} = \infty$.

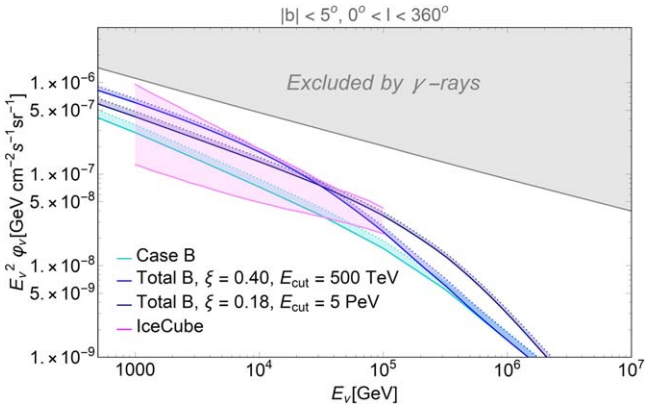

Figure 2. Differential energy spectra of the all-flavor diffuse neutrino emission from the Galactic region $|b| < 5^\circ$ and $0^\circ < l < 360^\circ$. The magenta region corresponds to the superposition of the three IceCube best fits for the Galactic component with their 1σ uncertainty. The predictions for the diffuse emission (Case B) and the total neutrino flux (Case B + sources) are shown with a cyan band and blue band, respectively. The bands represent the uncertainties on the spatial distributions of CRs in our Galaxy. The solid and dotted lines are obtained by assuming smearing radius infinity and 1 kpc, respectively. We show the effect of different energy cutoffs for the CR source spectra as displayed in the labels. We additionally display an excluded region in gray. The bottom line corresponds to the maximum neutrino contribution from our Galaxy obtained by assuming Case B for the diffuse emission, $\xi = 1$ and $E_{\mathrm{cut}} = \infty$.

almost the same constraints above ∼50 TeV. Moreover, in order to be conservative and to take into account the systematic uncertainty related to the adopted template, we show with the magenta region the superposition of the regions obtained by IceCube by using different assumptions (including also 1σ uncertainties of the respective fits). The displayed band shows that the energy region most effectively probed by IceCube is $50 \leqslant E_\nu \leqslant 100$ TeV since different assumptions basically lead to the same reconstructed flux. At lower energy, the extracted signal depends instead on the assumed neutrino spectrum. In this respect, we recall that the neutrino spectral index is assumed to be equal to 2.7 in the π_0 model, while it is close to 2.5 for the KRA_γ models. We finally note that the IceCube

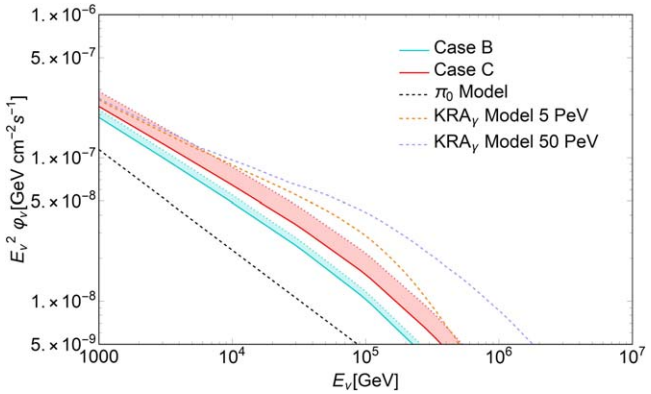

Figure 3. We compare the all-sky, single-flavor expectations provided by different models for the truly diffuse emission due to the CR interactions with the interstellar medium. The diffuse emission due to Case B and Case C are plotted with a blue and a red band, respectively. Predicted nominal values for the π_0, the KRA$_\gamma^5$, and the KRA$_\gamma^{50}$ are also displayed for a comparison.

signal is always below the maximal limit allowed by gamma-ray observations discussed in the previous paragraph (gray solid lines in Figures 2 and 1). This is a relevant conclusion, different from that obtained by ANTARES (Albert et al. 2023) that reported a hint for a Galactic neutrino signal that can extend well above this limit; see Vecchiotti et al. (2023).

The truly diffuse neutrino emission $\varphi_{\nu,\rm diff}$ due to CR interactions with the ISM is displayed by the cyan band in Figure 2, labeled as Case B, and by the red band in Figure 1, labeled as Case C. We calculate this contribution by following the prescriptions of Pagliaroli et al. (2016) and Cataldo et al. (2019); the details are reported in Appendix A. The main source of uncertainty for the calculation of this component is the determination of the differential CR flux $\varphi_{\rm CR}(E, \boldsymbol{r})$ as a function of the energy and position in the Galaxy. In our Case B, CRs are assumed to have the same spectrum in the entire Galaxy; the flux $\varphi_{\rm CR}(E, \boldsymbol{r})$ can be thus directly linked to its local determination $\varphi_{\rm CR,\odot}(E)$ parameterized by Dembinski et al. (2018) by a position-dependent normalization factor that is calculated by assuming isotropic diffusion from the (nonuniform) distributions of CR sources in the Galaxy. The obtained results depend on the adopted diffusion radius R. The upper limit (both for Case B and Case C subsequently discussed) is obtained by taking $R = 1$ kpc, i.e., by assuming that CRs are confined relatively close to their sources. The lower limit is obtained by assuming $R = \infty$ that corresponds to a CR spatial distribution very close to that predicted by the GALPROP code. Finally, Case C implements as an additional ingredient the possibility, recently emerged from the analysis of Fermi-LAT gamma-ray data at GeV energies (Acero et al. 2016; Yang et al. 2016; Pothast et al. 2018), that CRs have a harder spectrum in the inner Galaxy than at the Sun position; see Appendix A for details. As a result of these assumptions, one expects a larger neutrino emission in the TeV domain, with a harder spectral index (that also depends on the direction of the observation), as it is displayed by the red band in Figure 1.

Our predictions for the truly diffuse emission are compared with the three reference models used by IceCube in Figure 3. As it is expected, our Case C is very similar to the KRA$_\gamma^5$, while Case B predicts a diffuse emission, which is a factor $\sim$2 greater than the π_0 model. This is due to the fact that the π_0 model is obtained by extrapolating the neutrino diffuse emission at GeV energies (estimated from gamma-ray data) with a spectral index equal to 2.7. This is, however, not consistent with the observed CR spectral behavior that shows a hardening at rigidity $\sim$300 GV (Adriani et al. 2011; Aguilar et al. 2015a, 2015b). This feature is automatically implemented in our calculations but is not considered in the π_0 model that consequently underestimates neutrino diffuse emission.

The first conclusion that is obtained from our calculations is that the Galactic gamma-ray source population cannot be entirely powered by hadronic mechanisms. Indeed, the total predicted neutrino flux that is obtained by taking $\xi = 1$ greatly exceeds the IceCube signal both in Case B and Case C unless the proton cutoff energy is much lower than 100 TeV, i.e., a value that is not compatible with the fact that gamma-ray sources have been observed to emit up to sub-PeV energy domain; see e.g., (Abeysekara et al. 2020; Cao et al. 2023).

This conclusion is particularly strong and rich in physical implications when we consider our Case C, i.e., if we assume that the CR spectral index is position dependent and becomes harder toward the Galactic center, as obtained from the analysis of the Fermi-LAT data by Acero et al. (2016), Yang et al. (2016), and Pothast et al. (2018). Indeed, as it is reported in Figure 1, the diffuse emission in our Case C saturates the IceCube signal, leaving no space for any other additional contribution. This result is consistent with the best-fit normalization smaller than 1 that was obtained by the IceCube analysis for the KRA $^5_\gamma$ model (Abbasi et al. 2023). The above result automatically implies that the source contribution to the observed signal should be zero or negligible. In other words, one is forced to require that either $\xi \ll 1$ or $E_{\rm cut} \ll 500$ TeV in such a way that the source contribution in the energy range probed by IceCube becomes much smaller than the CR diffuse emission. This requirement, however, could be not easily fulfilled in the context of the model that we are considering. Indeed, CRs up to the proton knee energy are believed to have a Galactic origin. This implies the existence of sources in our Galaxy that should accelerate hadrons up to few PeV energy. As an example, the KRA$_\gamma^5$ model assumes that the source injection spectrum is a power law with an exponential cutoff at 5 PeV. In order to not exceed the IceCube signal, one is forced to assume that these sources accelerate hadrons up to few PeV but do not effectively produce neutrinos in the 1–100 TeV energy range.

The situation is quite different if we consider our Case B, i.e., we assume that the CR spectrum is uniform within the Galaxy and corresponds to that measured at the Earth and parameterized by Dembinski et al. (2018). In this case, the IceCube data allow for a non-vanishing source contribution that seems to be even required if we restrict the comparison to the most constrained energy range $50 \leqslant E_\nu \leqslant 100$ TeV.

The blue bands reported in Figure 2 show the total (diffuse + sources) neutrino emission evaluated by using Equation (1) and considering selected values of the two parameters ξ and $E_{\rm cut}$. We see that the allowed fraction ξ of TeV gamma-ray sources that can have hadronic nature depends on the assumed proton cutoff energy. If we require that Galactic sources accelerate protons up to the "knee" around $E_{\rm cut} = 5$ PeV (Lipari & Vernetto 2020), which could represent the end of the Galactic CR's component (Gabici et al. 2019), the maximal fraction is $\sim$20%, corresponding to a source contribution integrated between 1 and 100 TeV that is equal to $\Phi_{\nu,s} = 1.1 \times 10^{-10}\,{\rm cm}^{-2}\,{\rm s}^{-1}$. For a smaller cutoff energy $E_{\rm cut} = 500$ TeV, we obtain $\xi \leqslant 40\%$, corresponding to

$\Phi_{\nu,s} \leqslant 2.6 \times 10^{-10}\,\mathrm{cm}^{-2}\,\mathrm{s}^{-1}$. Larger values for ξ require smaller proton cutoff energies that, however, would correspond to the assumption that the neutrino (and gamma-ray) source emission spectrum is suppressed above few $\times$ 10 TeV, with potential difficulties to explain the IceCube signal in the most constrained energy region above 50 TeV. Finally, we can compare our findings with our present knowledge of TeV gamma-ray sources. If we consider the HGPS catalog, we obtain that the cumulative gamma-ray flux integrated in the 1–100 TeV energy range that is produced by potential hadronic sources, i.e., eight supernova remnants and eight composite sources, is about ∼12% of the total gamma-ray signal $\Phi_{\gamma,s} = 4.2 \times 10^{-10}\,\mathrm{cm}^{-2}\,\mathrm{s}^{-1}$ produced by the entire (resolved + unresolved) source population (see Table 1 of Cataldo et al. 2020). Converted in neutrinos, these 16 sources would account for a cumulative flux at a level of $\sim 6.0 \times 10^{-11}\,\mathrm{cm}^{-2}\,\mathrm{s}^{-1}$. This flux is not negligible and compatible with our limits for Case B, thus potentially confirming this scenario in which a comparable contribution to the IceCube signal is provided by diffuse and source components and disfavoring instead our Case C, which requires a negligible source contribution. However, the number of identified sources of this kind is still very limited, not allowing us to reach this conclusion on firm statistical grounds.

3. Summary

In conclusion, we have discussed the implications of the recent measurement of high-energy neutrino emission from the Galactic disk performed by IceCube. We have shown that the IceCube signal is compatible with the upper limit allowed by TeV gamma-ray observations calculated by Vecchiotti et al. (2023). Moreover, we have demonstrated that only a fraction of the TeV-Galactic gamma-ray sources can have hadronic nature. This fraction has to be negligible if we assume that CRs diffusing in the inner Galaxy have a spectrum harder than at the Sun position, as it is, e.g., assumed in the KRAγ models or, equivalently, in our Case C. This may not be compatible with the fact that these models require the existence of sources in our Galaxy that accelerate hadrons up to few PeV. Moreover, the observed gamma-ray sources with potential hadronic nature in the HGPS catalog (i.e., supernova remnants, SNRs, and composite sources) already account for a non-negligible flux ∼10% $\Phi_{\nu,\mathrm{s}}^{\mathrm{max}}$ when converted in neutrinos.

If we consider instead the standard scenario in which the CR spectrum is uniform within the Galaxy (i.e., Case B), the maximally allowed fraction is $\xi \leqslant 40\%$ for a cutoff energy of the source proton spectrum $E_{\mathrm{cut}} = 500$ TeV, corresponding to a cumulative source flux from the Galactic plane $\Phi_{\nu,\mathrm{s}} \leqslant 2.6 \times 10^{-10}\,\mathrm{cm}^{-2}\,\mathrm{s}^{-1}$. Lower cutoff energies are not consistent with the IceCube signal at ∼100 TeV, while larger cutoffs lead to smaller values for $\Phi_{\nu,\mathrm{s}}$. In particular, the fraction of hadronic Galactic sources compatible with IceCube results reduces to ∼20% for energy cutoff, reaching the cosmic-ray proton knee around 5 PeV.

Acknowledgments

The work of V.V. is supported by the European Research Council (ERC) under the ERC-2020-COG ERC Consolidator Grant (grant agreement No. 101002352). The work of G.P. and F.L.V. is partially supported by the research grant number 2017W4HA7S "NAT-NET: Neutrino and Astroparticle Theory Network" under the program PRIN 2017 funded by the Italian Ministero dell'Istruzione, dell'Universita'e della Ricerca (MIUR).

Appendix A
Neutrino Diffuse Emission

The neutrino diffuse flux is calculated following the approach of Pagliaroli et al. (2016) and Cataldo et al. (2019) that is summarized in the following. The differential one-flavor neutrino flux can be parametrized as

$$\varphi_{\nu,\mathrm{diff}}(E_\nu, \hat{n}_\nu) = \frac{1}{3} \sum_{l=e,\mu,\tau} \int_{E_\nu}^{\infty} dE\, \frac{d\sigma_l(E, E_\nu)}{dE_\nu} \times \int_0^{\infty} dl\, \varphi_{\mathrm{CR}}(E, r_\odot + l\hat{n}_\nu) n_{\mathrm{H}}(r_\odot + l\hat{n}_\nu), \quad \text{(A1)}$$

where E_ν and $\hat{n}_\nu$ indicate, respectively, the neutrino energy and arrival direction, while $\frac{d\sigma_l(E,E_\nu)}{dE_\nu}$ represents the differential cross section for the production of neutrino and antineutrino with flavor l by a nucleon of energy E in a nucleon–nucleon collision. In Equation (A1), the neutrino flux at Earth is assumed to be equally distributed among the different flavors due to neutrino mixing (see, e.g., Palladino et al. 2015). The nucleon–nucleon cross section is parameterized by using Kelner et al. (2006). The number density of target nucleons $n_{\mathrm{H}}(\boldsymbol{r})$ contained in the gas is taken from the GALPROP code[4] and includes the contributions from atomic H and molecular H_2 hydrogen (Moskalenko et al. 2002). We take into account the contribution of heavy elements by assuming that the total mass of the ISM is a factor 1.42 larger than the mass of hydrogen Ferriere (2001). The differential CR flux $\varphi_{\mathrm{CR}}(E, \boldsymbol{r})$ can be written as

$$\varphi_{\mathrm{CR}}(E, \boldsymbol{r}) = \varphi_{\mathrm{CR},\odot}(E) g(\boldsymbol{r}) h(E, \boldsymbol{r}), \quad \text{(A2)}$$

where $\varphi_{\mathrm{CR},\odot}(E)$ represents the local nucleon flux, which is described according to the data-driven parameterization provided in Dembinski et al. (2018).

The function $g(\boldsymbol{r})$ describes the spatial distribution of CRs and is an adimensional function (normalized to one at the Sun position $\boldsymbol{r}_\odot = 8.5$ kpc). It is obtained as the solution of a 3D isotropic diffusion equation with constant diffusion coefficient and stationary CR injection $f_{\mathrm{S}}(\boldsymbol{r})$:

$$g(\boldsymbol{r}) = \frac{1}{N} \int d^3x\, f_{\mathrm{S}}(\boldsymbol{r} - \boldsymbol{x}) \frac{\mathcal{F}(|\boldsymbol{x}|/R)}{2\pi|\boldsymbol{x}|}, \quad \text{(A3)}$$

where $f_{\mathrm{S}}(\boldsymbol{r})$ is assumed to follow the SNR number density parameterization given by Green (2015) and N is a normalization constant:

$$N = \int d^3x\, f_{\mathrm{S}}(\boldsymbol{r}_\odot - \boldsymbol{x}) \frac{\mathcal{F}(|\boldsymbol{x}|/R)}{2\pi|\boldsymbol{x}|}, \quad \text{(A4)}$$

while the function $\mathcal{F}(\delta)$ is defined as

$$\mathcal{F}(\delta) \equiv \int_\delta^\infty d\gamma\, \frac{1}{\sqrt{2\pi}} \exp(-\gamma^2/2). \quad \text{(A5)}$$

The solution depends on the diffusion length R, for which we assume two extreme values, $R = 1$ kpc and $R = \infty$, which allow us to reproduce the behavior of the CR density at

[4] GALPROP is made available at https://galprop.stanford.edu/.

$E \sim 20$ GeV obtained by analysis of Fermi-LAT data; see Cataldo et al. (2019) for details.

The function $h(E, \boldsymbol{r})$ introduces the possibility of a position-dependent CR spectral index as inferred from analysis of the Fermi-LAT data (see, e.g., Acero et al. 2016; Yang et al. 2016; Pothast et al. 2018), and it is defined as

$$h(E, \boldsymbol{r}) = \left(\frac{E}{\overline{E}}\right)^{\Delta(\boldsymbol{r})}, \tag{A6}$$

where $\overline{E} = 20$ GeV is the pivot energy and $\Delta(\boldsymbol{r}_\odot) = 0$. The function $\Delta(\boldsymbol{r})$ in Galactic cylindrical coordinates is modeled as

$$\Delta(r, z) = \Delta_0 \left(1 - \frac{r}{r_\odot}\right) \tag{A7}$$

for $r \leqslant 10$ kpc, while it is assumed to be constant for larger distances. The factor $\Delta_0 = 0.3$ represents the difference between the CR spectral index at the Galactic center and its value at the Sun position.

Appendix B
Total Gamma-Ray Source Flux

The cumulative gamma-ray source signal is calculated following the approach of Cataldo et al. (2020). The source spatial and luminosity distribution is described as

$$\frac{dN}{d^3r\, dL} = \rho(\boldsymbol{r})\, Y(L), \tag{B1}$$

where $\boldsymbol{r}$ indicates the source position and L is the source gamma-ray intrinsic luminosity in the 1–100 TeV energy range probed by the H.E.S.S. detector. The spatial distribution $\rho(\boldsymbol{r})$, normalized to 1 when integrated over the entire Galaxy, is proportional to the pulsar distribution parameterized by Lorimer et al. (2006) and scales as $\exp(-|z|/H)$ with $H = 0.2$ kpc, along the direction z perpendicular to the Galactic plane. The source luminosity function $Y(L)$ is described by

$$Y(L) = \frac{\mathcal{N}}{L_{\rm max}} \left(\frac{L}{L_{\rm max}}\right)^{-\alpha} \tag{B2}$$

in the luminosity range $L_{\rm min} \leqslant L \leqslant L_{\rm max}$. In the above relation, $L_{\rm max}$ and $\mathcal{N}$ are the maximum TeV gamma-ray luminosity of the population and the high-luminosity normalization of the luminosity function, respectively. The total TeV gamma-ray flux produced by all the sources (resolved and unresolved) in a given OW is calculated by using the prescription of Cataldo et al. (2020):

$$\Phi_{\gamma,{\rm s}} = \frac{\mathcal{N} F_{\rm max}}{4\pi(2 - \alpha)} \int_{\rm OW} d^3r\, \rho(\boldsymbol{r})\, r^{-2}, \tag{B3}$$

where $F_{\rm max} = L_{\rm max}/\langle E \rangle$ represents the maximum TeV emissivity, and $\langle E \rangle = 3.25$ TeV is the average energy of photons emitted in the range 1–100 TeV obtained by assuming that all the gamma-ray sources have a power-law spectrum with a spectral index equal to 2.3 (Abdalla et al. 2018). The best-fit value of $\mathcal{N}$ is not sensitive to a change in the spectral assumption, while $L_{\rm max}$ is shifted proportionally to the variation of $\langle E \rangle$. As a consequence, if the spectral assumption is changed, $F_{\rm max}$ remains constant and $\Phi_{\gamma,{\rm s}}$ is unchanged. Here, we use the best-fit values $L_{\rm max} = 5.1^{+3.4}_{-2.2} \times 10^{35}$erg s^{-1} and $\mathcal{N} = 18^{+14}_{-7}$ derived in Cataldo et al. (2020) for $\alpha = 1.5$ by fitting the flux, longitude, and latitude distributions of the sample of 32 HGPS sources above the H.E.S.S. completeness threshold.

Appendix C
Total Neutrino Source Flux

The neutrino source flux is obtained from the gamma-ray flux following the approach of Vecchiotti et al. (2023). The CR-injected spectrum is parameterized as a power law with an exponential cutoff $\phi_{\rm p}(E) \propto E^{-\Gamma_{\rm p}} \exp(-E/E_{\rm cut})$. The proton spectral index is fixed to $\Gamma_p = 2.4$ to reproduce the average spectral properties of HGPS sources. The proton cutoff energy varies in the range $E_{\rm cut} = 0.5$–10 PeV to explore the relevance of this parameter for our final results. The all-flavor neutrino spectrum (normalized in the 1–100 TeV energy window) produced by hadronic interaction within the source is given by

$$\phi_\nu(E_\nu; E_{\rm cut}) = \frac{1}{K_\nu(E_{\rm cut})} \sum_{l=e,\mu,\tau} \times \int_{E_\nu}^{\infty} dE \frac{d\sigma_l(E, E_\nu)}{dE_\nu} \phi_p(E; E_{\rm cut}), \tag{C1}$$

where $K_\nu(E_{\rm cut})$ is the normalization constant:

$$K_\nu(E_{\rm cut}) = \sum_{l=e,\mu,\tau} \int_{E_{\rm inf}}^{E_{\rm sup}} dE_\nu \times \int_{E_\nu}^{\infty} dE\, \frac{d\sigma_l(E, E_\nu)}{dE_\nu}\, \phi_p(E; E_{\rm cut}), \tag{C2}$$

where $E_{\rm inf} = 1$ TeV and $E_{\rm sup} = 100$ TeV. By using Equations (C1) and (B3), we calculate the cumulative neutrino emission produced by all sources (resolved and unresolved) contained in a given OW. The all-flavor differential neutrino flux is given by

$$\varphi_{\nu,s}(E_\nu; E_{\rm cut}, \xi) = \xi\, \Phi^{\rm max}_{\nu,{\rm s}}(E_{\rm cut})\, \phi_\nu(E_\nu; E_{\rm cut}), \tag{C3}$$

where $\Phi^{\rm max}_{\nu,{\rm s}} \equiv \eta\, \Phi_{\gamma,{\rm s}}$. The parameter η represents the ratio between the number of neutrinos (of all flavors) and the number of photons that a given source produces in the energy window 1–100 TeV, and it is defined as $\eta \equiv \frac{K_\nu}{K_\gamma}$, where

$$K_\gamma(E_{\rm cut}) = \int_{E_{\rm inf}}^{E_{\rm sup}} dE_\gamma \int_{E_\gamma}^{\infty} dE\, \frac{d\sigma(E, E_\gamma)}{dE_\gamma}\, \phi_p(E; E_{\rm cut}). \tag{C4}$$

The flux $\Phi^{\rm max}_{\nu,{\rm s}}$ represents the maximal neutrino source contribution, i.e., the one obtained by assuming that all the TeV gamma-ray sources, resolved and unresolved, are powered by hadronic processes. We introduce the quantity $\xi \leqslant 1$ to consider the possibility that only a fraction of the gamma-ray source flux is produced by hadronic interaction and hence is accompanied by neutrino production.

ORCID iDs

V. Vecchiotti https://orcid.org/0000-0002-9802-3678
F. L. Villante https://orcid.org/0000-0001-7667-4499
G. Pagliaroli https://orcid.org/0000-0002-6751-9996

References

Aartsen, M. G., Ackermann, M., Adams, J., et al. 2017, ApJ, 849, 67
Abbasi, R., Ackermann, M., Adams, J., et al. 2023, Sci, 380, 1338
Abdalla, H., Abramowski, A., Aharonian, F., et al. 2018, A&A, 612, A1
Abeysekara, A. U., Albert, A., Alfaro, R., et al. 2020, PhRvL, 124, 021102
Acero, F., Ackermann, M., Ajello, M., et al. 2016, ApJS, 223, 26
Ackermann, M., Ajello, M., Atwood, W. B., et al. 2012, ApJ, 750, 3
Adriani, O., Barbarino, G. C., Bazilevskaya, G. A., et al. 2011, Sci, 332, 69
Adrian-Martinez, S., Albert, A., André, M., et al. 2016, PhLB, 760, 143
Aguilar, M., Aisa, D., Alpat, B., et al. 2015a, PhRvL, 114, 171103
Aguilar, M., Aisa, D., Alpat, B., et al. 2015b, PhRvL, 115, 211101
Ahlers, M., & Murase, K. 2014, PhRvD, 90, 023010
Albert, A., André, M., Anghinolfi, M., et al. 2017, PhRvD, 96, 062001
Albert, A., André, M., Anghinolfi, M., et al. 2018, ApJL, 868, L20
Albert, A., Alfaro, R., Alvarez, C., et al. 2020, ApJ, 905, 76
Albert, A., Alves, S., André, M., et al. 2023, PhLB, 841, 137951
Cao, Z., Aharonian, F., An, Q., et al. 2023, arXiv:2305.17030
Cataldo, M., Pagliaroli, G., Vecchiotti, V., & Villante, F. L. 2019, JCAP, 12, 050
Cataldo, M., Pagliaroli, G., Vecchiotti, V., & Villante, F. L. 2020, ApJ, 904, 85
Dembinski, H. P., Engel, R., Fedynitch, A., et al. 2018, in Int. Cosmic Ray Conf., Proc. of Science, 35, 533
Evoli, C., Grasso, D., & Maccione, L. 2007, JCAP, 06, 003
Fang, K., & Murase, K. 2021, ApJ, 919, 93
Ferriere, K. M. 2001, RvMP, 73, 1031
Gabici, S., Evoli, C., Gaggero, D., et al. 2019, IJMPD, 28, 1930022
Gaggero, D., Grasso, D., Marinelli, A., Urbano, A., & Valli, M. 2015, ApJL, 815, L25
Green, D. 2015, MNRAS, 454, 1517
Kelner, S. R., Aharonian, F. A., & Bugayov, V. V. 2006, PhRvD, 74, 034018
Lipari, P., & Vernetto, S. 2018, PhRvD, 98, 043003
Lipari, P., & Vernetto, S. 2020, APh, 120, 102441
Lorimer, D. R., Faulkner, A. J., Lyne, A. G., et al. 2006, MNRAS, 372, 777
Moskalenko, I. V., Strong, A. W., Ormes, J. F., & Potgieter, M. S. 2002, ApJ, 565, 280
Pagliaroli, G., Evoli, C., & Villante, F. L. 2016, JCAP, 11, 004
Palladino, A., Pagliaroli, G., Villante, F. L., & Vissani, F. 2015, PhRvL, 114, 171101
Pothast, M., Gaggero, D., Storm, E., & Weniger, C. 2018, JCAP, 10, 045
Schwefer, G., Mertsch, P., & Wiebusch, C. 2023, ApJ, 949, 16
Vecchiotti, V., Pagliaroli, G., & Villante, F. L. 2022a, CmPhy, 5, 161
Vecchiotti, V., Zuccarini, F., Villante, F. L., & Pagliaroli, G. 2022b, ApJ, 928, 19
Vecchiotti, V., Villante, F. L., & Pagliaroli, G. 2023, JCAP, 2023, 027
Yang, R., Aharonian, F., & Evoli, C. 2016, PhRvD, 93, 123007